ACS APPLIED NANO MATERIALS

Article

Cite This: ACS Appl. Nano Mater. 2019, 2, 7214−7219

www.acsanm.org

Confinement Effects and Charge Dynamics in Zn_3N_2 Colloidal Quantum Dots: Implications for QD-LED Displays

Ruben Ahumada-Lazo,[†] Simon M. Fairclough,[‡,▽] Samantha J. O. Hardman,[§] Peter N. Taylor,[∥] Mark Green,[⊥] Sarah J. Haigh,[‡] Rinku Saran,[#,○] Richard J. Curry,[#] and David J. Binks*[,†]

[†]Department of Physics and Astronomy and the Photon Science Institute, [‡]Department of Materials, [§]Manchester Institute of Biotechnology, and [#]Photon Science Institute, Department of Electrical and Electronic Engineering, The University of Manchester, Manchester M13 9PL, U.K.

[∥]Sharp Laboratories of Europe Ltd, Edmund Halley Road, Oxford Science Park, Oxford OX4 4GB, U.K.

[⊥]Department of Physics, King's College London, Strand, London, U.K. WC2R 2LS

Supporting Information

ABSTRACT: Zinc nitride (Zn_3N_2) colloidal quantum dots are composed of nontoxic, low-cost, and earth-abundant elements. The effects of quantum confinement on the optical properties and charge dynamics of these dots are studied using steady-state optical characterization and ultrafast fluence-dependent transient absorption. The absorption and emission energies are observed to be size-tunable, with the optical band gap increasing from 1.5 to 3.2 eV as the dot diameter decreased from 8.9 to 2.7 nm. Size-dependent absorption cross sections (σ = 1.22 ± 0.02 × 10^{-15} to 2.04 ± 0.03 × 10^{-15} cm^2), single exciton lifetimes (0.36 ± 0.02 to 0.65 ± 0.03 ns), as well as Auger recombination lifetimes of biexcitons (3.2 ± 0.4 to 5.0 ± 0.1 ps) and trions (20.8 ± 1.8 to 46.3 ± 1.3 ps) are also measured. The degeneracy of the conduction band minimum (g = 2) is determined from the analysis of the transient absorption spectra at different excitation fluences. The performance of Zn_3N_2 colloidal quantum dots thus broadly matches that of established visible light emitting quantum dots based on toxic or rare elements, making them a viable alternative for QD-LED displays.

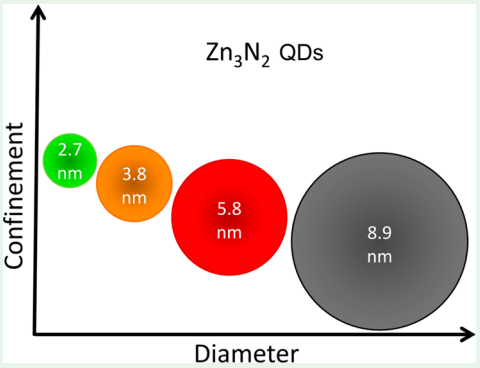

KEYWORDS: *quantum confinement, charge dynamics, zinc nitride, quantum dots, QD-LED*

INTRODUCTION

The size-tunable optical and electronic properties, photostability, and solution-based synthesis and processability of semiconductor nanocrystals, also known as colloidal quantum dots (QDs), have motivated research into their suitability for a wide variety of applications, such as photovoltaic cells,[1] photocatalysts,[2] light emitting devices,[3] and biosensors.[4] In particular, QD-LEDs have the potential to be the basis of high-performance displays, offering a wide color gamut, high contrast ratio, and the high resolution (pixel density) needed for mobile and automotive devices as well as the scalability needed for large-area display applications.[5] However, the most extensively studied and used QDs for these applications contain intrinsically toxic elements such as Cd and Pb, which is a concern due to the potential environmental and public health impact,[5,6] or rare elements such as In. In order to comply with increasingly stringent international standards and regulations without prohibitive cost, the exploration of alternative, Cd- and Pb-free, quantum dots made from commonly available elements is urgently needed.[5−7]

Zinc nitride (Zn_3N_2) is a nontoxic, low-cost, and earth-abundant semiconductor[8] that has not yet been exploited as much as group III nitrides because of the difficulties in the preparation of high-quality Zn_3N_2 crystals.[9] Studies of the structural, electrical, and optical properties of this material have been largely limited to thin film geometries, which have been prepared by a variety of methods including metal−organic chemical vapor deposition,[9] RF−molecular beam epitaxy,[9] direct reaction by annealing metallic zinc in an ammonia atmosphere,[10] pulsed laser ablation,[11] molten salt potentiostatic electrolysis of zinc,[12] as well as DC[13,14] and RF[15,16] magnetron sputtering. A wide range of optical bandgap values have been reported in these studies (varying from ∼1.0 to 3.2 eV), generating some controversy about the origin and true nature of the electronic transitions. A likely contributor to the confusion present in the literature is the tendency of Zn_3N_2 to oxidize rapidly in ambient conditions, as revealed by X-ray photoelectron spectroscopy (XPS),[15] spectroscopic ellipsometry, and Rutherford backscattering spectrometry (RBS).[16] A recent work comparing the optical properties of Zn_3N_2 films with different stoichiometries and oxidized films has revealed that the intrinsic bandgap of Zn_3N_2 is of a direct nature in the

Received: September 6, 2019
Accepted: October 28, 2019
Published: October 28, 2019

DOI: 10.1021/acsanm.9b01714
ACS Appl. Nano Mater. 2019, 2, 7214−7219

Scheme 1. Synthesis of Zn_3N_2 Colloidal Quantum Dots[a]

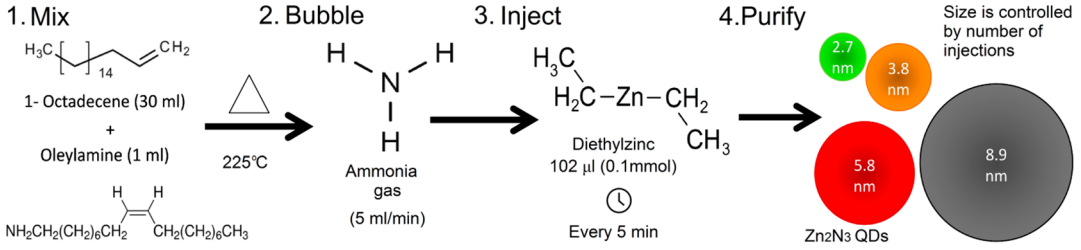

[a](1) In an inert atmosphere, a mixture of 1-octadecene and oleylamine is heated to 225°C. (2) Ammonia gas is bubbled through the solvent, and diethylzinc is rapidly injected at 5 min intervals. (3) Zn_3N_2 quantum dots size is controlled by the number of diethylzinc injections.

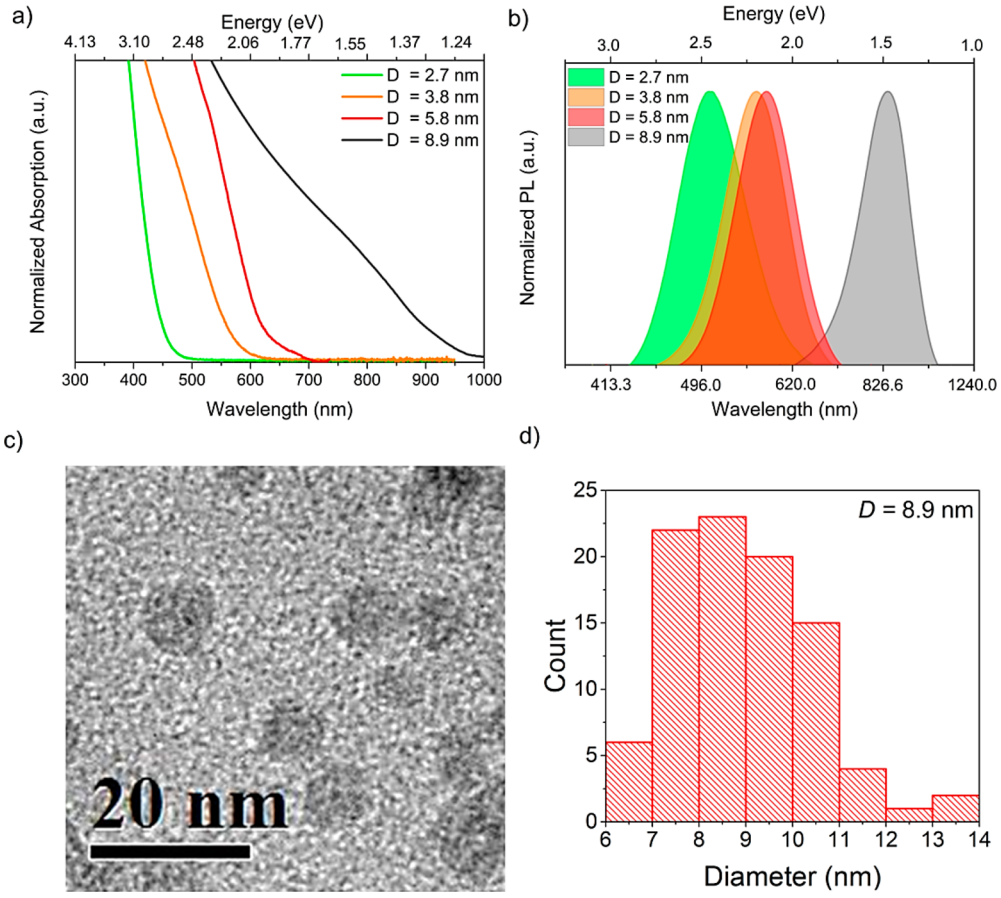

Figure 1. (a) Absorption and (b) PL spectra for Zn_3N_2 QDs of different sizes. PL was produced by excitation at a wavelength of 350 nm. (c) TEM image of the largest QDs. (d) Size frequency histogram for the same sample.

range from 1.31 to 1.48 eV, while the presence of the ZnO or $Zn_xO_yN_z$ phases formed on top of zinc nitride upon air exposure lead to much wider bandgaps.[13] However, the optical properties of different Zn_3N_2 samples have also been found to be related to inhomogeneities in surface roughness, defect-induced carrier concentrations, as well as oxidation.[9,13,16] Theoretical studies have calculated the bandgap to be in the ranges of 0.9 to 1.2 eV[17] and 0.84 to 2.0 eV,[18] which are both in broad agreement with experimental values. Perhaps due to difficulties in handling air sensitive materials with high intrinsic surface area, very few studies have reported the synthesis and properties of nanostructured Zn_3N_2 morphologies,[19,20] with only one work describing the synthesis (see Scheme 1) and optical properties of colloidal Zn_3N_2 QDs.[21] Importantly, this paper successfully demonstrated the tunability of the optical emission due to quantum confinement effects alongside high photoluminescent quantum yields (35−52%). The critical next step in the exploitation of this promising new type of colloidal quantum dot is to determine whether key properties are comparable to those of conventional quantum dots and thus establish it as a viable as well as nontoxic and earth-abundant alternative.

In this work, the optical properties of a series of Zn_3N_2 quantum dots of different sizes are characterized by transmission electron microscopy and steady-state absorption and photoluminescence (PL) spectroscopies. Ultrafast fluence-dependent transient absorption spectroscopy, supported by transient PL studies, is then used to investigate the charge dynamics at different excitation regimes. Knowledge of the size-dependent material properties determined in this work, such as the absorption cross section, the degeneracy of the conduction band minimum, the trapping rates, and Auger

DOI: 10.1021/acsanm.9b01714
ACS Appl. Nano Mater. 2019, 2, 7214−7219

recombination lifetimes are fundamental to the development of Cd- and Pb-free QD-LED displays and other devices such as photovoltaics and biosensors.

RESULTS AND DISCUSSION

Steady-state absorption and photoluminescence (PL) spectra for QDs of several different mean diameters, D, are shown in Figure 1. For each sample, the value of D and the standard deviation of the size distribution were found directly from transmission electron microscope (TEM) images as shown in Figure 1c,d, respectively, for the largest QDs (see Supporting Information for the other samples). Well-defined peaks are not evident in the absorption spectra (Figure 1a), and so, the position of the lowest energy absorbing transition for each sample was determined from the second derivative of these spectra, as detailed in the Supporting Information, and found to be at 3.2 ± 0.1 eV (380 ± 10 nm), 2.6 ± 0.1 eV (480 ± 20 nm), 2.3 ± 0.2 eV (540 ± 45 nm), and approximately 1.5 ± 0.1 eV (~840 ± 40 nm) for the 2.7 ± 0.6, 3.8 ± 0.8, 5.8 ± 0.9, and 8.9 ± 1.6 nm average diameter QDs, respectively. The relationship between the energy of this transition and D agrees well with a simple effective mass model of the band gap as discussed in Section S4 of the Supporting Information. Figure 1b shows the PL emission spectrum for each of these samples, which display maxima at 2.46 eV (505 nm), 2.20 eV (564 nm), 2.15 eV (578 nm), and 1.48 eV (840 nm). The optical band gap of Zn_3N_2 thin films has recently been reported to range between 1.31 and 1.48 eV,[13] suggesting that the largest diameter QDs (8.9 nm) are only subject to weak quantum confinement, if any. This is consistent with the calculated value for the exciton Bohr radius (a_B), which ranges from ~1 to ~3.8 nm depending on which values of effective mass and dielectric constant from the literature are used (see Table S1 in the Supporting Information).[9,11,13,18,22−24] The full-width half maxima (fwhm) of the PL spectra were 0.46 eV (95 nm), 0.41 eV (104 nm), 0.38 eV (103 nm), and 0.32 eV (180 nm), respectively, i.e., about 20% of the peak energy for each sample. This is in agreement with the polydispersity observed in the size frequency histograms and consistent with the lack of pronounced absorption peaks. Moreover, the samples show a highly size-dependent Stokes shift (following the trend observed in other types of QDs[25,26]), with differences between absorption and emission energies ranging from 20 to 740 meV, for the largest and smallest QDs, respectively. While these values may have a contribution from nonresonant absorption due to size dispersion, a resonant Stokes shift is likely to originate from quantum confinement effects on the band structure of semiconductors.[25] Stokes shifts on the order of those found here for the smaller nanoparticles have been reported for Zn_3P_2 QDs[27,28] and attributed to charges being trapped by metal vacancies.[28] Although its exact nature is yet to be understood in this material, large Stokes shifts indicate that Zn_3N_2 QDs could also make a good optical gain medium for QD lasing applications.[29]

An example contour plot showing the pump-induced absorption change, ΔA, spectra as a function of delay time is shown in Figure 2. Further examples for other QD diameters and for a range of pump pulse fluences, J_p, are given in the Supporting Information. The main feature in these plots is a strong and broad bleach (i.e., negative ΔA), which is centered at 500 nm in the spectra for the 3.8 nm diameter QDs as shown in Figure 2. The center wavelength of this feature closely agrees (within error) with the wavelength of the first minimum in the second derivative of the steady-state absorption spectra (this is also the case for the rest of the samples, with bleach features at 560 ± 40 and 840 ± 40 nm, for samples D = 5.8 and D = 8.9, respectively, as shown in the SI). The bleach is therefore attributed to state-filling at the conduction band minimum (CBM), in common with many other QD types.[30] A photoinduced absorption feature (PIA) (i.e., positive ΔA) at the same wavelengths at earlier times than the bleach is also evident. The duration of the PIA is similar to that of the pump pulse and so is attributed to a nonlinear response of the solvent.

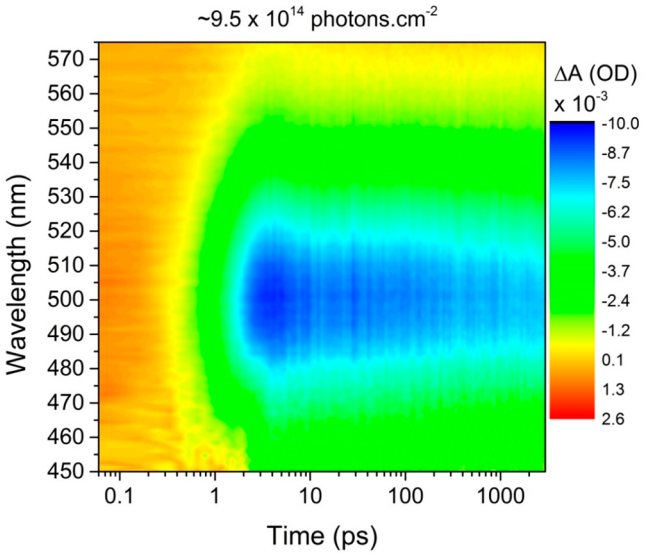

Figure 2. Pump-induced transient absorption spectra for the 3.8 nm average diameter QDs excited by 100 fs pulses with a wavelength of 380 nm and fluence of 9.5 × 10^{14} photons·cm^{-2}. Contour plot shows the change in absorption, ΔA, as a function of wavelength and delay time, where a negative value of ΔA (green and blue) demonstrates a bleach effect.

Figure 3 shows the maximum fractional bleach, $\Delta A/A$, as a function of J_p for the 3.8 nm diameter QD sample at a wavelength of 500 nm (the center of the absorption bleach).

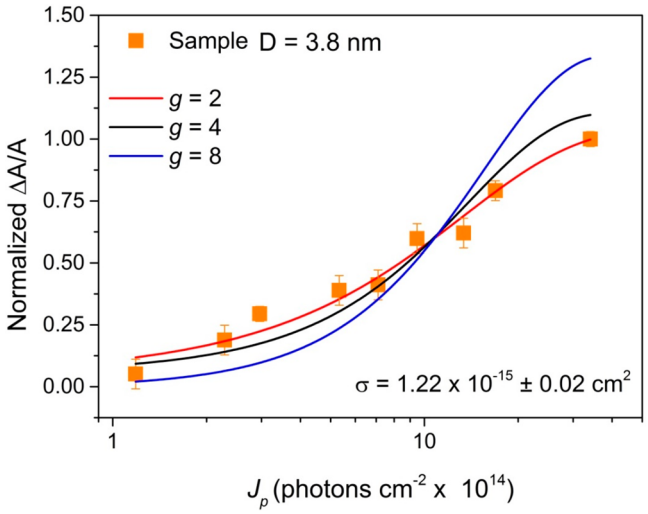

Figure 3. Normalized peak in $\Delta A/A$ at a wavelength of 500 nm as a function of pump pulse fluence for sample with diameter D = 3.8 nm. Fits are to eq 1 for different values of CBM degeneracy, g.

DOI: 10.1021/acsanm.9b01714
ACS Appl. Nano Mater. 2019, 2, 7214−7219

The value of $\Delta A/A$ for a CBM bleach produced by state-filling in QDs depends on the degeneracy of the CBM, g, and the average number of photons absorbed per QD per pulse, $\langle N \rangle = J_p\sigma$, where σ is the absorption cross section at the pump wavelength.[31] This relationship is given by

$$\frac{\Delta A(\langle N\rangle)}{A} = (1 - P_0(\langle N\rangle)) - \sum_{i=1}^{g}\left(\frac{g-1}{g}\right)P_i(\langle N\rangle) \quad (1)$$

where $P_i = \langle N\rangle^i e^{-\langle N\rangle}/i!$ is the Poissonian probability of a QD absorbing i photons. Figure 3 shows fits of eq 1 for g = 2, 4, and 8; the data is best described by g = 2. This indicates that the CBM of Zn_2N_3 QDs is twofold degenerate, which is in common with many other QD types[31] including other II−V group QDs.[29] This fit also yields a value of $\sigma = (1.22 \pm 0.02) \times 10^{-15}$ cm^2. This is similar in magnitude to that for InAs QDs of similar size[32] (but in the strong confinement regime due to its much larger Bohr radius[33]), larger than the absorption cross section reported for InP QDs (6.9×10^{-16} cm^2) with a mean diameter of 4.2 nm,[34] and about an order of magnitude smaller than those for $CsPbBr_3$ perovskites ($\sigma = 1.3 \times 10^{-14}$ cm^2) emitting at similar wavelengths as this sample.[31] All of these materials have cross sections smaller than CdS QDs for which $\sigma \approx 1 \times 10^{-13}$ cm^2 was calculated for samples with 2.7 nm average diameter.[35] No values of absorption cross sections for other II−V QDs were found in the literature. A similar fit to the data for the 5.8 and 8.9 nm average diameter QDs is shown in Figure S6 in the Supporting Information and gave corresponding values of $\sigma = (1.3 \pm 0.3) \times 10^{-15}$ and $\sigma = (2.04 \pm 0.03) \times 10^{-15}$ cm^2, respectively. For strong confinement (i.e., $D \leq 2a_B$, where a_B is the exciton Bohr radius), σ typically scales linearly with the volume of the QD, but the value plateaus for larger nanocrystals as quantum confinement weakens.[31,36] Thus, this modest increase in σ as the QD diameter increases from 3.8 to 8.9 nm is also consistent with a small value of a_B, for Zn_3N_2 as discussed above. Using these values for absorption cross section and the measured steady-state absorbance, the concentration of the samples was calculated to be in the order of 1×10^{-9} mol·cm^3.

Figure 4 shows the fractional absorption change $\Delta A/A$ transients at the center of the absorption bleach feature (500 nm) for different $\langle N\rangle$ values, calculated from the excitation fluences using the cross section value extracted from the fit in Figure 3 (sample D = 3.8 nm). Similar data for the samples with QD diameters of 5.8 and 8.9 nm are shown in the Supporting Information. For low $\langle N\rangle$ values, excited QDs only contain single excitons, and their decay can be fitted by a monoexponential decay function plus a constant offset, corresponding to the effects of trapping and radiative recombination (which occurs over a longer time scale than the experimental time window), respectively.[37] The value of the associated time constant, τ_1^{TA}, is 0.36 ± 0.02 ns (0.39 ± 0.03 and 0.65 ± 0.03 ns for the samples with 5.8 and 8.9 nm diameter, respectively) and corresponds to the lifetime of single excitons in QDs with traps. This time constant is also present as τ_1^{PL} in the triexponential fit of the photoluminescence decay for this sample shown in Figure S8b. With the increase of excitation fluence, the probability of a single QD absorbing more than one photon per pulse increases, and the shape of the transients changes to that of a biexponential decay. This is consistent with the decay of biexcitons by Auger recombination in those QDs that absorb more than one photon per QD per pulse. By fixing one of the time constants in a biexponential fit to the τ_1^{TA} value obtained at low $\langle N\rangle$, the lifetimes for Auger recombination of biexcitons, τ_2^{TA}, can be reliably extracted, yielding a value of 3.2 ± 0.4 ps for the 3.8 nm diameter QDs (3.4 ± 0.5 and 5.0 ± 0.1 ps for the sample with 5.8 and 8.9 nm diameter). The reported biexciton lifetime for Cd_3P_2, another material from the II−V group, is 3.6 ps (D = 2.58 nm),[29] while values of 3.5 and 6.3 ps have been reported for CdS QDs with diameters of 3.1 and 3.4 nm, respectively. The biexciton lifetime also increases linearly with QD volume for strong confinement, increasing to 42 and 57 ps for CdS QDs of D = 4.7 nm and D = 4.9 nm, respectively, for instance. The more modest increase observed here for Zn_3N_2QDs as D increases from 3.8 to 8.9 nm is consistent with weak confinement.

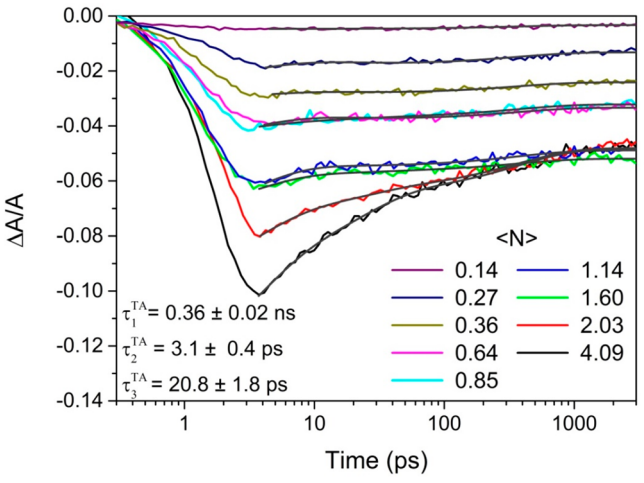

Figure 4. Fractional absorption change $\Delta A/A$ transients taken at a wavelength of 500 nm, at different excitation fluences ($\langle N\rangle$) for the sample with a 3.8 nm average diameter. Triexponential fits to the decays are shown as black lines.

Fluence-dependent $\Delta T/T$ measurements on nanocrystalline $ZnO_{0.51}N_{0.49}$ thin films,[38] fitted by a biexponential decay function, gave fast time constants ranging from 3.5 to 8.7 ps and a slow time constant with values between 45 and 115 ps. Both of these time constants become shorter as the excitation fluence is increased. Based on the analysis of the amplitudes of these time constants, the authors attribute them to the Auger recombination of biexcitons at high fluences and trapping of charges at low fluences, respectively.

For higher excitation fluences, ($\langle N\rangle > 1$), a third time constant, τ_3^{TA}, is required to fit the decays. For the D = 3.8 nm sample, a τ_3^{TA} value of 20.8 ± 1.8 ps was extracted from the triexponential fits by fixing the other two time constants to the values obtained at lower pump fluences; τ_3^{TA} values of 24.2 ± 2.5 and 46.3 ± 1.3 ps were found for the D = 5.8 nm and D = 8.9 nm samples, respectively. For other QD types,[39−41] a third decay channel that emerges at high $\langle N\rangle$ values but with a lifetime in between that for single exciton and biexciton decay has been associated with the Auger recombination of trions. These trions form when a photogenerated charge is trapped for a period longer than that between pump pulses so that its geminate charge is still present in the QD when a photon is absorbed during a subsequent excitation pulse.

CONCLUSIONS

The effects of quantum confinement on the optical properties and charge dynamics of a series of Zn_3N_2 colloidal quantum

DOI: 10.1021/acsanm.9b01714
ACS Appl. Nano Mater. 2019, 2, 7214−7219

dots were investigated by optical characterization and ultrafast fluence-dependent transient absorption. The absorption onsets and emission energies were shown to be size-dependent and widely tunable in the visible and near-infrared regions of the spectrum. The absorption cross section and recombination lifetimes of single excitons, biexcitons, and trions produced at different excitation regimes as well as the degeneracy of the conduction band minimum are all comparable to those of QDs of similar materials. Thus, we demonstrate promising optoelectronic performance from a Cd- and Pb-free QD system based on earth-abundant and low-cost elements. This new understanding of the transient optical properties for Zn_3N_2 colloidal quantum dots will contribute toward the development of optoelectronic devices based on nontoxic QDs, particular ones that rely on broad tunability across the visible spectrum, such as QD-LEDs for display technologies. In particular, we consider that future work could employ surface modification or passivation methods to optimize the stability and charge dynamics of these QDs.

EXPERIMENTAL SECTION

Colloidal Quantum Dots Synthesis. Zn_3N_2QDs were prepared using the solution-based method previously reported by Taylor et al.[21] All nanocrystals were prepared in a nitrogen atmosphere glovebox and handled using standard air-free methods. All solvents were thoroughly degassed and anhydrous before use. Briefly, a mixture of 1-octadecene and oleylamine (in a ratio of 30:1 mL) is heated to 225 °C, while 5 mL per minute of NH_3 gas is bubbled through the solvent. Diethylzinc is rapidly injected into the reaction mixture in portions of 102 μL and 1.0 mmol in 5 min intervals. The size of the QDs is controlled by the number of diethylzinc injections, which makes the dots grow with no signs of nucleation of additional nanocrystals. In a typical purification, the reaction mixture was centrifuged to remove any insoluble material. The resulting solution was then treated with anhydrous toluene, isobutyronitrile, and acetonitrile. The mixture was further centrifuged, the top layer was discarded, and the QDs were redispersed in nonpolar solvent such as toluene. This purification procedure was performed twice. Such obtained samples could be stored for several months under N_2 atmosphere in a glovebox.

Characterization. Samples for transmission electron microscopy (TEM) were drop cast on AGAR Scientific 400 mesh continuous carbon coated Cu support grids. Air exposure was minimized on loading by mounting the samples in the holder in argon baths and flooding the specimen airlock with argon before insertion. TEM images were acquired using a FEI Tescan F30 operating at 300 kV or JEOL F300 running at 200 kV.

The samples were placed in 10 mm path length airtight quartz cuvettes and diluted with anhydrous toluene under N_2 atmosphere in a glovebox prior to optical characterization. Steady-state absorbance and photoluminescence (PL) spectra were obtained using a Cary 5000 Agilent and a Horiba Jobin−Yvon FluoroLog iHR (FL33−22) spectrometers, respectively.

The transient absorption data were acquired using a previously described system,[42] comprising a Helios (Ultrafast Systems LLC) spectrometer, an ultrafast Ti:sapphire amplifier system (Spectra Physics Solstice Ace), and an optical parametric amplifier (Topas Prime) with an associated NIR−UV−vis unit. This system generated 100 fs pump pulses at 375 nm with a beam diameter of 240 μm. The pulse energy could be reduced using a series of reflective neutral density filters to give pump fluences from 1×10^{14} to 3.5×10^{15} photons·per cm^2 per pulse. A white light continuum generated by the same laser system that was used as the probe was used to record changes in absorption between 430 and 913 nm. The samples were magnetically stirred to avoid photocharging effects during the measurements. Steady-state absorbance spectra were acquired periodically to monitor and account for changes in absorbance due to oxidation of the Zn_3N_2 QDs.

ASSOCIATED CONTENT

Supporting Information

The Supporting Information is available free of charge on the ACS Publications website at DOI: 10.1021/acsanm.9b01714.

TEM images and size frequency histograms, second derivative of the absorption spectra, literature values for dielectric constant, electron and hole effective masses, transient absorption spectra and transient photoluminescence measurements, plot of band gap as a function of size, and Fourier transforms of TA decays (PDF)

AUTHOR INFORMATION

Corresponding Author

*E-mail: david.binks@manchester.ac.uk. (D.J.B.)

ORCID

Ruben Ahumada-Lazo: 0000-0002-1524-9576
Mark Green: 0000-0001-7507-1274
Sarah J. Haigh: 0000-0001-5509-6706
Richard J. Curry: 0000-0001-8859-5210
David J. Binks: 0000-0002-9102-0941

Present Addresses

[▽]Cambridge Centre for Gallium Nitride, University of Cambridge, Cambridge CB3 0FS, United Kingdom. (S.M.F.)
[○]Nanoscience Technology Center, University of Central Florida, Orlando, Florida 32826, United States. (R.S.)

Author Contributions

The manuscript was written through contributions of all authors. All authors have given approval to the final version of the manuscript.

Notes

The authors declare no competing financial interest.

ACKNOWLEDGMENTS

Transient absorption measurements were performed at the Ultrafast Biophysics Facility, Manchester Institute of Biotechnology, as funded by BBSRC Alert14 Award BB/M011658/1. R.A.-L. thanks CONACYT for provision of the scholarship 284566/399936. This work was supported by EPSRC awards EP/M015513/2, EP/P009050/1, and EP/M015653/1. S.J.H. and S.M.F. acknowledge funding from the European Research Council (ERC) under the European Union's Horizon 2020 research and innovation program (Grant Agreement ERC-2016-STG-EvoluTEM-715502). The data associated with this paper are openly available from Mendeley data: https://data.mendeley.com/datasets/mybsmj875j/1.

REFERENCES

(1) Clark, P. C. J.; Neo, D. C. J.; Ahumada-Lazo, R.; Williamson, A. I.; Pis, I.; Nappini, S.; Watt, A. A. R.; Flavell, W. R. Influence of Multistep Surface Passivation on the Performance of PbS Colloidal Quantum Dot Solar Cells. *Langmuir* **2018**, *34* (30), 8887−8897.

(2) Zhu, J.; Zäch, M. Nanostructured Materials for Photocatalytic Hydrogen Production. *Curr. Opin. Colloid Interface Sci.* **2009**, *14* (4), 260−269.

(3) Davis, N. J. L. K.; de la Peña, F. J.; Tabachnyk, M.; Richter, J. M.; Lamboll, R. D.; Booker, E. P.; Wisnivesky Rocca Rivarola, F.; Griffiths, J. T.; Ducati, C.; Menke, S. M.; Deschler, F.; Greenham, N. C. Photon Reabsorption in Mixed CsPbCl3: CsPbI3 Perovskite Nanocrystal Films for Light-Emitting Diodes. *J. Phys. Chem. C* **2017**, *121* (7), 3790−3796.

DOI: 10.1021/acsanm.9b01714
ACS Appl. Nano Mater. 2019, 2, 7214−7219

(4) Harvie, A. J.; Smith, C. T.; Ahumada-Lazo, R.; Jeuken, L. J. C.; Califano, M.; Bon, R. S.; Hardman, S. J. O.; Binks, D. J.; Critchley, K. Ultrafast Trap State-Mediated Electron Transfer for Quantum Dot Redox Sensing. *J. Phys. Chem. C* **2018**, *122*, 10173−10180.
(5) Smeeton, T. M.; Angioni, E.; Boardman, E. A.; Izumi, M.; Iwata, N.; Nakanishi, Y.; Ishida, T. Development of Electroluminescent QD-LED Displays. *Dig. Tech. Pap. - Soc. Inf. Disp. Int. Symp.* **2019**, *50* (1), 742−745.
(6) Hildebrandt, N.; Spillmann, C. M.; Algar, W. R.; Pons, T.; Stewart, M. H.; Oh, E.; Susumu, K.; Díaz, S. a.; Delehanty, J. B.; Medintz, I. L. Energy Transfer with Semiconductor Quantum Dot Bioconjugates: A Versatile Platform for Biosensing, Energy Harvesting, and Other Developing Applications. *Chem. Rev.* **2017**, *117*, 536−711.
(7) Tchounwou, P. B.; Yedjou, C. G.; Patlolla, A. K.; Sutton, D. J. Heavy Metal Toxicity and the Environment. *Molecular, Clinical and Environmental Toxicology* **2012**, *101*, 133−164.
(8) Coronel, N. C. *Earth-Abundant Zinc-IV-Nitride Semiconductors*, Ph.D. Thesis. California Insitute of Technology, 2016.
(9) Suda, T.; Kakishita, K. Band-Gap Energy and Electron Effective Mass of Polycrystalline Zn3N2. *J. Appl. Phys.* **2006**, *99* (7), 076101.
(10) Kuriyama, K.; Takahashi, Y.; Sunohara, F. Optical Band Gap of Zn3N2 Films. *Phys. Rev. B: Condens. Matter Mater. Phys.* **1993**, *48* (4), 2781−2782.
(11) Ayouchi, R.; Casteleiro, C.; Santos, L.; Schwarz, R. RF-Plasma Assisted PLD Growth of Zn3N2 Thin Films. *Phys. Status Solidi Curr. Top. Solid State Phys.* **2010**, *7* (9), 2294−2297.
(12) Toyoura, K.; Tsujimura, H.; Goto, T.; Hachiya, K.; Hagiwara, R.; Ito, Y. Optical Properties of Zinc Nitride Formed by Molten Salt Electrochemical Process. *Thin Solid Films* **2005**, *492* (1−2), 88−92.
(13) Trapalis, A.; Heffernan, J.; Farrer, I.; Sharman, J.; Kean, A. Structural, Electrical, and Optical Characterization of as Grown and Oxidized Zinc Nitride Thin Films. *J. Appl. Phys.* **2016**, *120* (20), 205102.
(14) Trapalis, A.; Farrer, I.; Kennedy, K.; Kean, A.; Sharman, J.; Heffernan, J. Temperature Dependence of the Band Gap of Zinc Nitride Observed in Photoluminescence Measurements. *Appl. Phys. Lett.* **2017**, *111* (12), 122105.
(15) Yang, T.; Zhang, Z.; Li, Y.; Lv, M. S.; Song, S.; Wu, Z.; Yan, J.; Han, S. Structural and Optical Properties of Zinc Nitride Films Prepared by Rf Magnetron Sputtering. *Appl. Surf. Sci.* **2009**, *255* (6), 3544−3547.
(16) García Núñez, C.; Pau, J. L.; Hernández, M. J.; Cervera, M.; Piqueras, J. On the True Optical Properties of Zinc Nitride. *Appl. Phys. Lett.* **2011**, *99* (23), 232112.
(17) Yoo, S. H.; Walsh, A.; Scanlon, D. O.; Soon, A. Electronic Structure and Band Alignment of Zinc Nitride, Zn 3N2. *RSC Adv.* **2014**, *4* (7), 3306−3311.
(18) Kumagai, Y.; Harada, K.; Akamatsu, H.; Matsuzaki, K.; Oba, F. Carrier-Induced Band-Gap Variation and Point Defects in Zn3N2 from First Principles. *Phys. Rev. Appl.* **2017**, *8* (1), 014015.
(19) Zong, F.; Ma, H.; Xue, C.; Du, W.; Zhang, X.; Xiao, H.; Ma, J.; Ji, F. Structural Properties of Zinc Nitride Empty Balls. *Mater. Lett.* **2006**, *60* (7), 905−908.
(20) Zong, F.; Ma, H.; Ma, J.; Du, W.; Zhang, X.; Xiao, H.; Ji, F.; Xue, C. Structural Properties and Photoluminescence of Zinc Nitride Nanowires. *Appl. Phys. Lett.* **2005**, *87* (23), 233104.
(21) Taylor, P. N.; Schreuder, M. A.; Smeeton, T. M.; Grundy, A. J. D.; Dimmock, J. A. R.; Hooper, S. E.; Heffernan, J.; Kauer, M. Synthesis of Widely Tunable and Highly Luminescent Zinc Nitride Nanocrystals. *J. Mater. Chem. C* **2014**, *2* (22), 4379−4382.
(22) Cao, X.; Yamaguchi, Y.; Ninomiya, Y.; Yamada, N. Comparative Study of Electron Transport Mechanisms in Epitaxial and Polycrystalline Zinc Nitride Films. *J. Appl. Phys.* **2016**, *119* (2), 025104.
(23) Yamada, N.; Watarai, K.; Yamaguchi, T.; Sato, A.; Ninomiya, Y. Transparent Conducting Zinc Nitride Films. *Jpn. J. Appl. Phys.* **2014**, *53* (5S1), 05FX01.
(24) Zervos, M.; Karipi, C.; Othonos, A. Zn3N2 Nanowires: Growth, Properties and Oxidation. *Nanoscale Res. Lett.* **2013**, *8*, 221.
(25) Demchenko, D. O.; Wang, L. Optical Transitions and Nature of Stokes Shift in Spherical CdS Quantum Dots. *Phys. Rev. B: Condens. Matter Mater. Phys.* **2006**, *73*, 155326.
(26) Brennan, M. C.; Zinna, J.; Kuno, M. Existence of a Size-Dependent Stokes Shift in $CsPbBr_3$ Perovskite Nanocrystals. *ACS Energy Lett.* **2017**, *2* (7), 1487−1488.
(27) Ho, M. Q.; Esteves, R. J. A.; Kedarnath, G.; Arachchige, I. U. Size-Dependent Optical Properties of Luminescent Zn3P2 Quantum Dots. *J. Phys. Chem. C* **2015**, *119* (19), 10576−10584.
(28) Green, M.; O'Brien, P. A Novel Metalorganic Route to Nanocrystallites of Zinc Phosphide. *Chem. Mater.* **2001**, *13* (12), 4500−4505.
(29) Wu, K.; Liu, Z.; Zhu, H.; Lian, T. Exciton Annihilation and Dissociation Dynamics in Group II-V Cd3P2 Quantum Dots. *J. Phys. Chem. A* **2013**, *117* (29), 6362−6372.
(30) Klimov, V. I. Spectral and Dynamical Properties of Multiexcitons in Semiconductor Nanocrystals. *Annu. Rev. Phys. Chem.* **2007**, *58* (1), 635−673.
(31) Makarov, N. S.; Guo, S.; Isaienko, O.; Liu, W.; Robel, I.; Klimov, V. I. Spectral and Dynamical Properties of Single Excitons, Biexcitons, and Trions in Cesium-Lead-Halide Perovskite Quantum Dots. *Nano Lett.* **2016**, *16* (4), 2349−2362.
(32) Yu, P.; Beard, M. C.; Ellingson, R. J.; Ferrere, S.; Curtis, C.; Drexler, J.; Luiszer, F.; Nozik, A. J. Absorption Cross-Section and Related Optical Properties of Colloidal InAs Quantum Dots. *J. Phys. Chem. B* **2005**, *109* (15), 7084−7087.
(33) Banin, U.; Lee, J. C.; Guzelian, a a; Kadavanich, a V; Alivisatos, a P. Exchange Interaction in InAs Nanocrystal Quantum Dots. *Superlattices Microstruct.* **1997**, *22* (4), 559−568.
(34) Ellingson, R. J.; Blackburn, J. L.; Yu, P.; Rumbles, G.; Mićić, O. I.; Nozik, A. J. Excitation Energy Dependent Efficiency of Charge Carrier Relaxation and Photoluminescence in Colloidal InP Quantum Dots. *J. Phys. Chem. B* **2002**, *106* (32), 7758−7765.
(35) Kobayashi, Y.; Nishimura, T.; Yamaguchi, H.; Tamai, N. Effect of Surface Defects on Auger Recombination in Colloidal CdS Quantum Dots. *J. Phys. Chem. Lett.* **2011**, *2* (9), 1051−1055.
(36) Castañeda, J. A.; Nagamine, G.; Yassitepe, E.; Bonato, L. G.; Voznyy, O.; Hoogland, S.; Nogueira, A. F.; Sargent, E. H.; Cruz, C. H. B.; Padilha, L. A. Efficient Biexciton Interaction in Perovskite Quantum Dots under Weak and Strong Confinement. *ACS Nano* **2016**, *10* (9), 8603−8609.
(37) Smith, C. T.; Leontiadou, M. A.; Page, R.; O'Brien, P.; Binks, D. J. Ultrafast Charge Dynamics in Trap-Free and Surface-Trapping Colloidal Quantum Dots. *Adv. Sci.* **2015**, *2* (10), 1500088.
(38) Shin, T.; Lee, E.; Sul, S.; Lee, H.; Ko, D.-S.; Benayad, A.; Kim, H.-S.; Park, G.-S. Ultrafast Photocarrier Dynamics in Nanocrystalline ZnO_xN_y Thin Films. *Opt. Lett.* **2014**, *39* (17), 5062−5065.
(39) Yarita, N.; Tahara, H.; Ihara, T.; Kawawaki, T.; Sato, R.; Saruyama, M.; Teranishi, T.; Kanemitsu, Y. Dynamics of Charged Excitons and Biexcitons in CsPbBr3 Perovskite Nanocrystals Revealed by Femtosecond Transient-Absorption and Single-Dot Luminescence Spectroscopy. *J. Phys. Chem. Lett.* **2017**, *8* (7), 1413−1418.
(40) Cadirci, M.; Stubbs, S. K.; Fairclough, S. M.; Tyrrell, E. J.; Watt, A. A. R.; Smith, J. M.; Binks, D. J. Ultrafast Exciton Dynamics in Type II ZnTe-ZnSe Colloidal Quantum Dots. *Phys. Chem. Chem. Phys.* **2012**, *14* (39), 13638−13645.
(41) Ahumada-Lazo, R.; Alanis, J. A.; Parkinson, P.; Binks, D. J.; Hardman, S. J. O.; Griffiths, J. T.; Wisnivesky Rocca Rivarola, F.; Humphrey, C. J.; Ducati, C.; Davis, N. J. L. K. Emission Properties and Ultrafast Carrier Dynamics of CsPbCl3 Perovskite Nanocrystals. *J. Phys. Chem. C* **2019**, *123*, 2651−2657.
(42) Brandariz-De-Pedro, G.; Heyes, D. J.; Hardman, S. J. O.; Shanmugam, M.; Jones, A. R.; Weber, S.; Nohr, D.; Scrutton, N. S.; Fielding, A. J. Direct Evidence of an Excited-State Triplet Species upon Photoactivation of the Chlorophyll Precursor Protochlorophyllide. *J. Phys. Chem. Lett.* **2017**, *8* (6), 1219−1223.

DOI: 10.1021/acsanm.9b01714
ACS Appl. Nano Mater. 2019, 2, 7214−7219